

Development of predictive pharmacophore model for in silico screening, and 3D QSAR CoMFA and CoMSIA studies for lead optimization, for designing of potent tumor necrosis factor alpha converting enzyme inhibitors

Prashant Revan Murumkar · Vishal Prakash Zambre ·
Mange Ram Yadav

Received: 24 August 2009 / Accepted: 9 February 2010 / Published online: 24 February 2010
© Springer Science+Business Media B.V. 2010

Abstract A chemical feature-based pharmacophore model was developed for Tumor Necrosis Factor- α converting enzyme (TACE) inhibitors. A five point pharmacophore model having two hydrogen bond acceptors (A), one hydrogen bond donor (D) and two aromatic rings (R) with discrete geometries as pharmacophoric features was developed. The pharmacophore model so generated was then utilized for in silico screening of a database. The pharmacophore model so developed was validated by using four compounds having proven TACE inhibitory activity which were grafted into the database. These compounds mapped well onto the five listed pharmacophoric features. This validated pharmacophore model was also used for alignment of molecules in CoMFA and CoMSIA analysis. The contour maps of the CoMFA/CoMSIA models were utilized to provide structural insight for activity improvement of potential novel TACE inhibitors. The pharmacophore model so developed could be used for in silico screening of any commercial/in house database for identification of TACE inhibiting lead compounds, and the leads so identified could be optimized using the developed CoMSIA model. The present work highlights the tremendous potential of the two mutually complementary ligand-based drug designing techniques (i.e. pharmacophore mapping and 3D-QSAR analysis) using TACE inhibitors as prototype biologically active molecules.

Keywords Pharmacophore model · In-silico screening · 3D-QSAR · TACE inhibitors

Introduction

Tumor Necrosis Factor-Alpha Converting Enzyme (TNF- α convertase, TACE) is a zinc metalloenzyme that catalyses the hydrolysis of Ala-Val bond of membrane-bound 233 residue 26 kDa pro-TNF- α , releasing soluble 17 kDa immunoregulating cytokine (tumour necrosis factor-alpha, TNF- α) into the circulation [1]. TNF- α is a very important proinflammatory mediator that is overproduced in inflammatory diseases such as rheumatoid arthritis (RA), multiple sclerosis, diabetes, ulcerative colitis and Crohn's disease, and congestive heart failure [2]. TNF- α and its receptors are over-expressed in the synovium and cartilage-pannus junction of RA joints [3]. Monoclonal antibodies against TNF- α (e.g. infliximab or Remicade) as well as soluble TNF- α receptor-Fc dimer (etanercept or Enbrel), although highly expensive, have become impressive anti-inflammatory agents in patients with RA [4]. Therapeutic effects of anti-TNF- α proteins last only for a short time due to their unfavourable pharmacokinetic profiles, therefore small orally bioavailable TACE inhibitors could have enormous potential as new therapeutics.

Ligand-based drug designing approaches like pharmacophore mapping and quantitative structure–activity relationship (QSAR) are used in drug discovery process in several ways, e.g. rationalisation of activity trends in molecules under study, prediction of the activity of novel compounds, database search studies for new hits and to identify important structural features for activity [5, 6]. The TACE enzyme was purified and cloned in 1997, a crystal structure was published in 1998 featuring large

P. R. Murumkar · V. P. Zambre · M. R. Yadav (✉)
Pharmacy Department, Faculty of Technology and Engineering,
The M. S. University of Baroda, Vadodara, Gujarat 390 001,
India
e-mail: mryadav11@yahoo.co.in

connected S1'-S3' sub sites [7], and quite a number of TACE inhibitors were pursued in the past [8]. The most advanced compound (BMS-561392/DPC-333) entered Phase II clinical trials in 2001 for rheumatoid arthritis and was also investigated for potential treatment of inflammatory bowel disease. Later it was withdrawn because of liver toxicity [9]. Although structure-based drug designing by using the 3D-structure of the target protein is an attractive drug designing strategy, a ligand-based approach like 3D-pharmacophore generation is useful for identifying the pharmacophoric features which could help in designing new molecules [10]. In a rational drug design approach, identification of the pharmacophore is the most important step in achieving the stipulated goal. For designing of novel newer potential TACE inhibitors, research work is in progress in this laboratory [11–16]. In our efforts towards finding potent TACE inhibitors, it was thought of gaining further insight into the structural requirements of TACE inhibitors by developing a pharmacophore model. Till date such a model of TACE inhibitors has remained unexplored. This paper describes the development of a robust ligand-based 3D-pharmacophore model for TACE inhibitors using Pharmacophore Alignment and Scoring Engine (PHASE) [17] software. The pharmacophore model so developed provides information about important structural features and their geometry in molecules for TACE inhibitory activity. The developed model has the ability to mine potential TACE inhibitors from 3D-virtual databases of drug-like molecules for the purpose of their in silico screening of TACE inhibitors. The conformations of active compounds obtained from the alignment of pharmacophoric points are used to derive CoMFA and CoMSIA 3D-QSAR models. The contour maps generated from 3D-QSAR studies could be of immense help for further designing of more potent inhibitors.

Experimental section

Data set

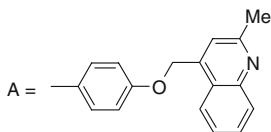
Over the last few years, a number of classes of TACE inhibitors have been identified. A set of 486 molecules having TACE inhibitory activity was collected from the literature [18–29]. Compounds with defined stereochemistry and well defined biological activity only were selected, excluding the recemates and those compounds which were reported to have biological activity less than or more than a particular value. Although, porcine TACE (pTACE) and human TACE both have quite high homology [21, 22] but due to the higher abundance of biological data on pTACE

and for the purpose of uniformity, compounds evaluated on pTACE only were included in the study. On the above described bases, a set of 220 compounds were considered for the pharmacophore generation. The in vitro bioactivities of the inhibitors so selected, were reported to be expressed as the concentration of the test compounds that inhibited pTACE by 50% (IC_{50}). To avoid redundancy of information, the data set was further refined by removing compounds with similar biological activity and chemical structures. On the basis of structural variations and differences in the biological activity, ultimately 80 compounds (Fig. 1, Table 1) with IC_{50} values ranging from 0.066 to 17,000 nM were used in the study [18–29]. The IC_{50} values (in moles/litre) was converted into negative logarithm of IC_{50} (pIC_{50}). For carrying out pharmacophore and CoMFA/CoMSIA 3D-QSAR studies, these 80 compounds were divided into training (61) and test (19) compounds with the following two rules: (a) both training and test set compounds were represented from each class of compounds to ensure structural diversity [if one class had only one compound, it was assigned to the training set (e.g., compound 80)]; (b) both, training and test sets covered the bioactivities (IC_{50}) as wide as possible. If there was only one compound with maximum or minimum order of bioactivity in a class, such a compound was assigned to the training set.

Pharmacophore model generation, validation and in silico screening of data base

Generation of common pharmacophore hypothesis

The development of common pharmacophore hypothesis (CPH) and alignment based on it were carried out using PHASE [17], version 2.5 (Schrodinger, LLC, New York, NY) installed on an SGI workstation. Structures of the 61 compounds of the training set were imported from the project table in the “Develop Pharmacophore Model” panel and geometrically refined (cleaned) using Ligprep module. Conformations were generated by the mixed MCMM/LMOD method using a maximum of 2,000 steps with a distance-dependent dielectric solvent model and an OPLS-2005 force field. All the conformers were subsequently minimised using truncated Newton conjugate gradient minimisation up to 500 iterations. For each molecule, a set of conformers with a maximum energy difference of 15 kcal/mol relative to the global energy minimum conformer were retained. A redundancy check of 2 Å in the heavy atom positions was applied to remove duplicate conformers. Pharmacophore features—hydrogen bond acceptor (A), hydrogen bond donor (D),



hydrophobic group (H), negatively charged group (N), positively charged group (P) and aromatic ring (R) were defined by a set of chemical structure patterns

 Springer

Table 1 Compounds used in the study and their IC₅₀ values (nM)

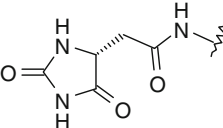
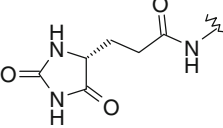
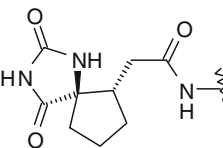
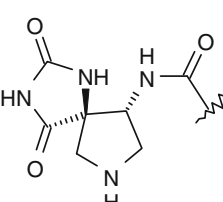
ID	X	R	Biological activity				
			Observed		Predicted (pIC ₅₀)		
			IC ₅₀ (nM)	pIC ₅₀	Phase (CPH1)	CoMFA	CoMSIA
1 ^a	CH ₂	–	1.00	9.000	9.08	9.495	9.213
2	CF ₂	–	6.30	8.200	8.26	8.171	8.023
3 ^a	N–C(O)OCH ₃	–	1.00	9.000	9.03	9.357	9.321
4 ^a	N- <i>i</i> -Pr	–	0.40	9.392	9.42	8.857	9.013
5 ^a (T)	N-Allyl	–	0.94	9.026	8.95	8.834	8.974
6 ^a	N-2-Propynyl	–	0.14	9.853	9.77	9.372	9.387
7 ^a	O	–	1.00	9.000	9.07	8.823	8.875
8 ^a (T)	CH ₂	–	1.00	9.000	7.91	7.892	7.928
09	NH	Me	2.2	8.656	8.64	8.715	8.654
10 ^a (T)	NCH ₂ C≡CH	Me	1.0	9.000	8.36	8.354	8.378
11	–	Me	6.0	8.221	8.17	8.425	8.314
12 ^a	–	Et	1.0	9.000	9.03	8.871	8.912
13 (T)	–	<i>i</i> -Pr	3.2	8.494	7.48	7.42	7.899
14 ^a	–	Cyclopropyl	1.0	9.000	8.98	8.885	8.912
15	–	Et	2.0	8.698	8.74	8.849	9.012
16	–	<i>t</i> -Bu	2.8	8.552	8.57	8.848	8.124
17 ^a	–	CF ₃	1.0	9.000	8.89	9.026	9.127
18 ^a	N-BOC	Me	1.0	9.000	9.01	9.060	8.951
19	NH	Me	2.6	8.585	8.59	8.716	8.613
20 ^a	O	CF ₃	1.0	9.000	8.98	9.343	9.214
21	–	<i>i</i> -Pr	1.1	8.958	8.91	8.895	8.913
22 (T)	–	<i>t</i> -Bu	2.0	8.696	8.95	8.983	8.876
23	–	CF ₂ CH ₃	2.6	8.585	8.59	8.576	8.736
24 ^b		–	170	6.769	6.75	6.528	6.635
25 ^b (T)		–	150	6.823	8.01	7.985	7.845
26		–	11	7.958	7.89	8.111	7.824
27		–	25	7.602	7.62	7.625	7.618

Table 1 continued

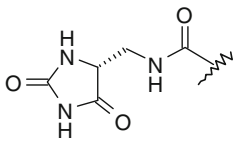
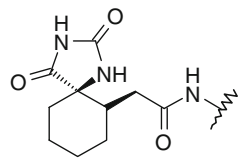
ID	X	R	Biological activity				
			Observed		Predicted (pIC ₅₀)		
			IC ₅₀ (nM)	pIC ₅₀	Phase (CPH1)	CoMFA	CoMSIA
28		—	98	7.008	7.11	7.417	7.297
29 ^b		—	900	6.045	6.12	6.135	6.126
30 ^b	—	—	294	6.531	6.52	6.765	6.523
31 (T)	—	—	55	7.239	7.86	7.913	7.896
32	NBoc	—	36	7.443	7.61	7.336	7.397
33	NH	—	92	7.036	7.01	6.943	7.098
34	N-Propyl	—	9.9	8.004	7.96	7.816	7.934
35	NH	—	43	7.366	7.32	7.392	7.386
36 (T)	CH ₂	—	2.5	8.602	7.78	7.83	7.941
37	CH ₂	—	8.6	8.065	8.05	8.183	8.179
38 (T)	NH	—	4.9	8.309	9.05	9.153	9.107
39	N-Propyl	—	11	7.958	7.94	8.125	8.109
40	N-Methyl	—	3.1	8.508	8.39	8.352	8.369
41	N ⁴ -Bu	—	3.7	8.431	8.40	8.425	8.429
42	N-(CH ₃) ₂ COOH	—	3.2	8.494	8.51	8.682	8.610
43	N-CH ₂ CH ₂ F	—	2.6	8.585	8.71	8.624	8.513
44	N-C(O)CH ₂ Bu	—	1.9	8.721	8.81	8.706	8.714
45 (T)	N-C(O)NMe ₂	—	2.8	8.552	8.20	8.195	8.267
46 ^b	—	Me	1,030	5.987	6.78	6.729	6.534
47 (T)	—	4- <i>n</i> -Hex-piperazin-1-yl	81	7.091	7.35	7.365	7.342
48 ^b	—	Piperazin-1-yl	1,100	5.958	6.34	6.459	6.437
49	—	4-Me-piperazin-1-yl	91	7.040	6.62	6.508	6.497
50 ^b	—	4-Bn-piperazin-1-yl	195	6.709	6.66	6.530	6.541
51	—	4[Ph(CH ₂) ₂]-piperazin-1-yl	84	7.075	7.13	7.170	6.953
52 ^b	—	4-(4-NO ₂ -Ph)-piperazin-1-yl	2,800	5.552	5.68	5.532	5.536
53 ^b	—	4-Ac-piperazin-1-yl	620	6.202	6.23	6.354	6.349
54 ^b (T)	—	4-Boc-piperazin-1-yl	160	6.795	6.78	6.984	6.864
55 ^b	—	—	7,300	5.136	5.01	5.168	5.163
56	—	—	8.00	8.096	8.15	7.512	7.834
57 ^a (T)	—	Cyclopropanecarbonyl	1.00	9.00	9.08	9.324	9.124
58 ^a	—	2-Furoyl	0.066	10.180	10.000	10.181	10.184
59 ^a	—	Cyclopropane cabonyl	0.45	9.346	9.56	9.685	9.679
60 ^a	—	Methanesulfonyl	0.48	9.318	9.37	9.013	9.125
61 ^a (T)	—	Methoxycarbonyl	0.28	9.552	9.47	9.489	9.493
62	—	Cyclobutyl	1.60	8.795	8.78	7.822	7.633
63 ^a	—	—	1.00	9.00	9.09	8.632	8.798
64 ^a	—	—	1.00	9.00	9.47	7.762	7.782

Table 1 continued

ID	X	R	Biological activity				
			Observed		Predicted (pIC ₅₀)		
			IC ₅₀ (nM)	pIC ₅₀	Phase (CPH1)	CoMFA	CoMSIA
65 ^b	–	–	140	6.853	6.84	6.913	6.901.8
66 (T)	–	–	7.00	8.154	8.18	8.143	8.103
67 (T)	–	–	26	7.858	7.79	7.697	7.703
68 ^b	–	–	111	6.954	6.87	6.882	6.893
69 ^b	–	Methoxy	887	6.052	6.47	6.459	6.323
70	–	Allyloxy	97	7.013	6.70	6.693	6.698
71	–	Benzyloxy	4	8.397	8.37	8.145	8.213
72 ^b (T)	–	Phenyl	13,000	4.886	6.87	6.832	6.793
73	–	3-Nitrobenzyloxy	6	8.221	8.41	8.826	8.712
74 (T)	–	3,5-di-MeO-benzyloxy	7	8.154	8.23	8.234	8.241
75	–	3,5-Bis-CF ₃ -benzyloxy	2	8.698	8.65	8.831	8.856
76	–	(Pyridine-4-yl)methoxy	21	7.677	7.72	7.216	7.318
77	–	(Quinolin-4-yl)methoxy	1.8	8.744	8.73	8.565	8.569
78 ^a (T)	–	(2-Me-quinolin-4-yl)methoxy	1	9.00	8.05	8.154	8.132
79 ^b	–	H	2,200	5.657	5.75	5.972	5.875
80 ^b	–	–	162	6.790	6.75	7.003	6.875

T test set

^a Active compound, ^b inactive compound

Point: The site is located on a single atom in the SMARTS query.

Vector: The site is located on a single atom in the SMARTS query, and assigned directionality according to one or more vectors originating from the atom.

Group: The site is located at the centre of a group of atoms in the SMARTS query. For aromatic rings, the site is assigned directionality, defined by a vector that is normal to the plane of the ring.

Active and inactive thresholds of pIC₅₀ of 9.00 and 7.00 respectively, were applied to the dataset of the above obtained 80 compounds to yield 21 actives and 17 inactives (Table 1) that were used for pharmacophore generation and subsequent scoring. Compounds having activity ≥ 9.00 were considered as active compounds and those having ≤ 7.00 were considered as inactive. Common pharmacophoric features were then identified from a set of variants - a set of feature types that define a possible pharmacophore - using a tree-based partitioning algorithm with maximum tree depth of four with the requirement that all 21 actives must match. The final size of the pharmacophore box was fixed at 1 Å to optimise the number of final CPHs. These five CPHs were examined using a scoring function to yield the best alignment of the active ligands using an overall maximum root mean square deviation (RMSD) value of 1.2 Å with default options for distance tolerance. The quality of alignment was measured by a survival score (S), defined as:

$$S = W_{\text{site}}S_{\text{site}} + W_{\text{vec}}S_{\text{vec}} + W_{\text{vol}}S_{\text{vol}} + W_{\text{sel}}S_{\text{sel}} + W_{\text{rew}}^m - W_E\Delta E + W_{\text{act}}A$$

where, W's are weights and S's are scores; S_{site} represents alignment score, the RMSD in the site point position; S_{vec} represents vector score, and averages the cosine of the angles formed by corresponding pairs of vector features in aligned structures; S_{vol} represents volume score based on overlap of van der Waals models of nonhydrogen atoms in each pair of structures; and S_{sel} represents selectivity score, and accounts for what fraction of molecules are likely to match the hypothesis regardless of their activity towards the receptor. W_{site} , W_{vec} , W_{vol} have default values of 1.0, while W_{sel} has a default value of 0.0. In hypothesis generation, default values have been used. The reward comes in the form of W_{rew}^m , where W_{rew} is user-adjustable (1.0 by default) and m is the number of actives that match the hypothesis minus one. $W_E\Delta E$ represents penalty included for high-energy structures by subtracting a multiple of the relative energy from the final score and penalize hypothesis for which the reference ligand activity is lower than the highest activity, by adding a multiple of the reference ligand activity to the score represented by $W_{\text{act}}A$, where A is the activity.

Assessment of CPH using partial least square analysis

A training set of 61 molecules were selected as described earlier, incorporating biological and chemical diversity,

and was used to generate atom-based QSAR models for all of the generated hypotheses using a grid spacing of 1.0 Å. Models containing six or more partial least squares (PLS) factors tended to fit the pIC_{50} values beyond their experimental uncertainty, therefore only one to five factor models were considered. Each of these models was validated using an external test set of 19 molecules that were not considered during model generation. The CPH with best predictive value and satisfactory statistics (i.e. CPH1) was chosen for alignment of molecules and used for further 3D-QSAR studies.

Pharmacophore models containing three, four and five sites were generated using a terminal box size of 1 Å with 21 highly active molecules, belonging to different chemical classes, using a tree based partition algorithm. The three- and four-featured Common Pharmacophore Hypotheses (CPHs) were rejected, as they were unable to define the complete binding space of the selected molecules. A total of 699 probable five-featured CPHs belonging to 14 types (AA-ADD, AAADH, AAADR, AAAHR, AAARR, AADDH, AADDR, AADHR, AADRR, AAHRR, ADDHR, ADDRR, ADHRR and DDHRR) were subjected to stringent scoring function analysis with respect to actives using default parameters for site, vector, and volume. Reference relative conformational energy (kJ/mol) was included in the score with a weight of 0.01, and ligand activity, expressed as pIC_{50} , with a weight of 1.0. Hypotheses emerging from this process were subsequently scored with respect to the 17 inactives, using a weight of 1.0. The hypotheses that survived the scoring process were used to build an atom-based QSAR model in PHASE. Training set molecules were aligned on these CPH and analysed by PLS analysis described in PHASE with 5 PLS components. Over-fitting of results was observed when more than 5 PLS components were analysed. The predictivity of each hypothesis was analysed by test set molecules. A summary of statistical data of the best five CPHs, labelled CPH1 to CPH5, with their survival scores is listed in Table 2. More consistent external predictivity was

observed for CPH1 for each combination as compared to the others.

Superimposition of pharmacophore features on the active site of TACE

Since crystal structure of pTACE is not available in PDB, hTACE (pdb code: 2fv5) was used for performing superimposition studies. The hTACE structure (pdb code: 2fv5, chain B) obtained from Protein Data Bank (PDB, USA) was used for the superimposition of the pharmacophore features because after performing BLAST-2 search [31] with porcine TACE, it was observed that sequence of human TACE has high degree of homology with that of pTACE (highest identity/BLAST Score) [12]. The sequence of the 839 amino acids of the pTACE was retrieved from the Swiss-Port Database [32].

Use and validation of the generated pharmacophore model for in silico screening

The generated pharmacophore model was used to carry out a search for potential TACE inhibitors of the ASINEX (<http://zinc.docking.org/vendor0/asin/index.html> asin_p0.0.sdf) database version 2006.3, # in catalog: 372187, made up of 45,533 molecules. Four highly active molecules and two inactives (Fig. 2) for TACE inhibitory activity were planted from outside in the database. The minimum criteria for retrieval of hits was that all the five out of five pharmacophoric features must match, with default tolerance on matching the pharmacophore features to each of the five inter-feature distances. The molecules were minimised using Ligprep module and a maximum of 100 conformers were generated for each molecule using the ligand torsional search method.

CoMFA and CoMSIA interaction energy calculations

Molecular modeling, CoMFA and CoMSIA analysis were performed using SYBYL 7.0 software running on Silicon Graphics Fuel workstation [30]. The steric and electrostatic fields were calculated at each lattice intersection of a regularly spaced grid of 2.0 Å in all the three dimensions within a defined region. The van der Waals potentials and Coulombic terms representing the steric and electrostatic fields, respectively, were calculated using standard Tripos force fields. A distance-dependent dielectric constant of 1.00 was used. An sp^3 carbon atom with +1.0 charge was used as a probe atom. The steric and electrostatic fields were truncated at +30.0 kcal/mol.

In CoMSIA interaction energy calculations, the steric, electrostatic, hydrophobic, hydrogen bond donor and hydrogen bond acceptor potential fields were calculated at

Table 2 Summary of PLS analysis results for the best five common pharmacophore hypotheses (CPHs) with survival scores

CPH	Survival score	SD	r_{ncv}^2	F	RMSE	r_{cv}^2
1	2.831	0.1363	0.9926	1243.7	0.7681	0.5925
2	2.543	0.0796	0.9958	2264.2	0.8325	0.4797
3	2.597	0.1388	0.9872	738.3	0.802	0.5171
4	2.627	0.1308	0.9886	832.8	0.880	0.4186
5	2.543	0.1864	0.9771	383.2	0.8896	0.4085

Bold values indicate the model having the best statistical figures when compared to other developed models

SD standard deviation of the regression, r_{ncv}^2 r -squared non cross validated, F variance ratio, RMSE root-mean-squared error, r_{cv}^2 r -squared cross validated

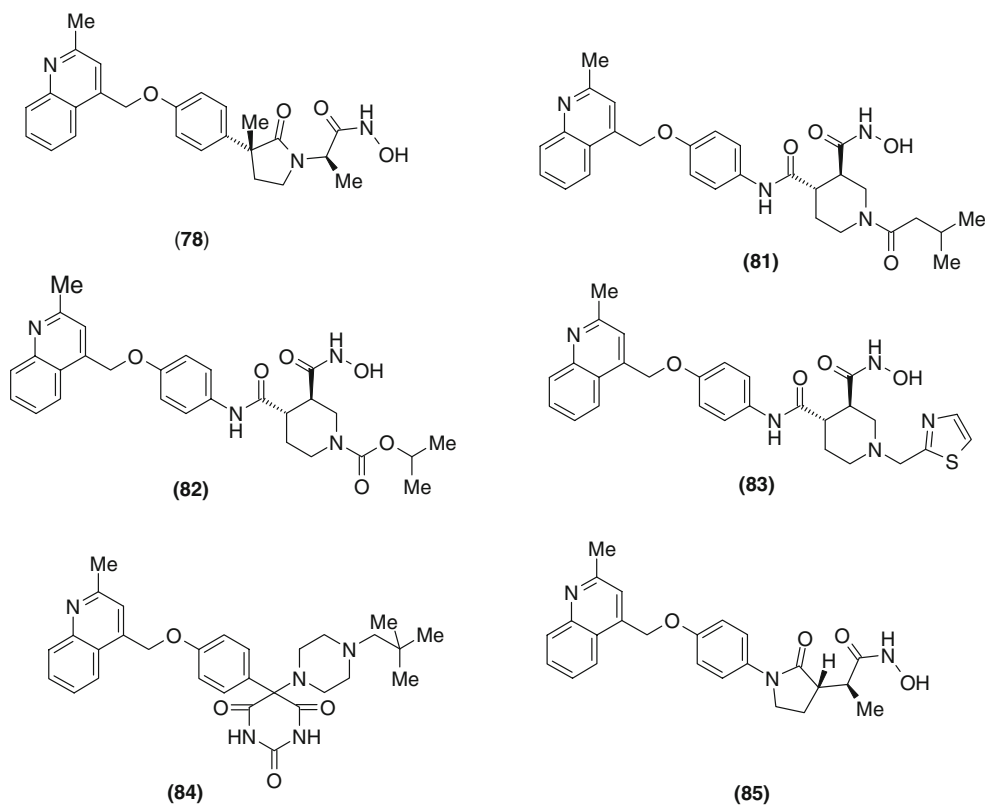


Fig. 2 Chemical structures of four active (**78**, **81–83**) and two inactive (**84**, **85**) TACE inhibitors used for validation of in silico screening method

each lattice intersection of a regularly spaced grid of 2.0 Å. A probe atom with radius 1.0 Å and +1.0 charge with hydrophobicity of +1.0 and hydrogen bond donor and hydrogen bond acceptor properties of +1.0 were used to calculate steric, electrostatic, hydrophobic donor and acceptor fields. The contribution from these descriptors was truncated at 0.3 kcal/mol.

Results and discussion

Out of the five pharmacophore models developed using PHASE, CPH1 showed excellent r^2 value for the training set (0.9926) and good predictive power with r_{cv}^2 of 0.5925. Actual and predicted values of the training set and test set molecules are given in the Table 1.

The pharmacophore contains two aromatic ring features, one mapping on the central phenyl ring and the other on the phenyl part of the quinoline ring, as shown in Fig. 3, two acceptor features, one mapping on the lone pair of oxygen of central carbonyl of the amide group and the other mapping on oxygen of the carbonyl group of the hydroxamate, and one hydrogen donor, NH of the hydroxamate moiety (Fig. 3). The distances and angles among the pharmacophoric features are depicted in Fig. 4a, b, respectively.

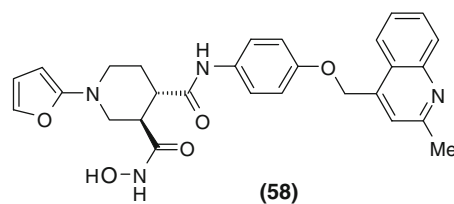
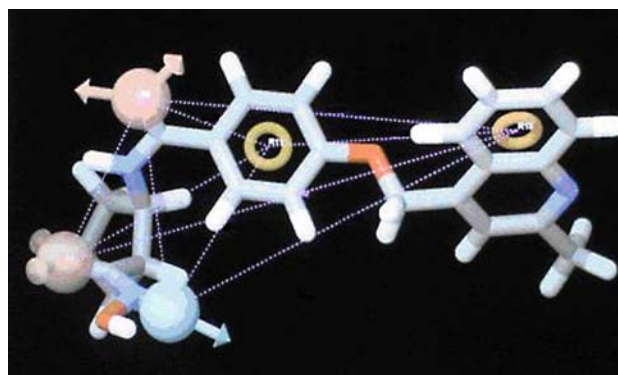


Fig. 3 Mapping of active compound (**58**) on the pharmacophore features (CPH1)

As crystal structure of hTACE is available, the superimposition of pharmacophore features on the active site has been carried out to further assess the compatibility of generated pharmacophore features (two aromatic rings, two

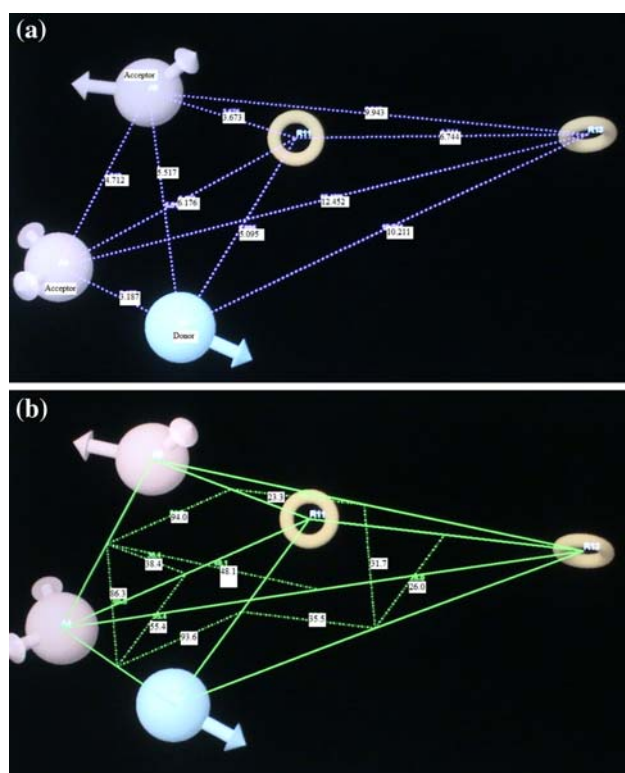


Fig. 4 Geometry of the pharmacophore (CPH1). *Red spheres with vectors* acceptor feature, *orange torus* aromatic ring features, *blue sphere* donor features **a** distances **b** angles

acceptors and one donor) with the active site as shown in Fig. 5. The first aromatic ring representing the P1' group accommodates the S1' subsite of the enzyme. Second aromatic ring acts as a linker between zinc binding group and the P1' side chain. The third and fourth, acceptor and donor features lie in the vicinity of Leu348 and Gly349 residuals respectively, further confirming that this acceptor and donor region is important to have a bonding with the NH group of Leu348 and CO of Gly349. The fifth pharmacophore feature i.e. acceptor is aligned towards the zinc motif (Fig. 5a, b). Thus, the identified pharmacophore features are in perfect consonance with the active site of hTACE.

The developed pharmacophore model (CPH1) was used for in silico screening of ASINEX data base for potential compounds possessing TACE inhibitory activity. In order to validate the screening protocol, four active and two inactive molecules were grafted into the data base. The four active molecules **78** (IK682), **81**, **82** and **83** having TACE inhibitory activity and two inactives, **84** and **85** were taken from the literature [18–20]. Figure 1 shows the chemical structures of these compounds. The in silico screening process retrieved 453 positive hits along with the above said four grafted active molecules and filtered out the two grafted inactives [32]. This clearly authenticated

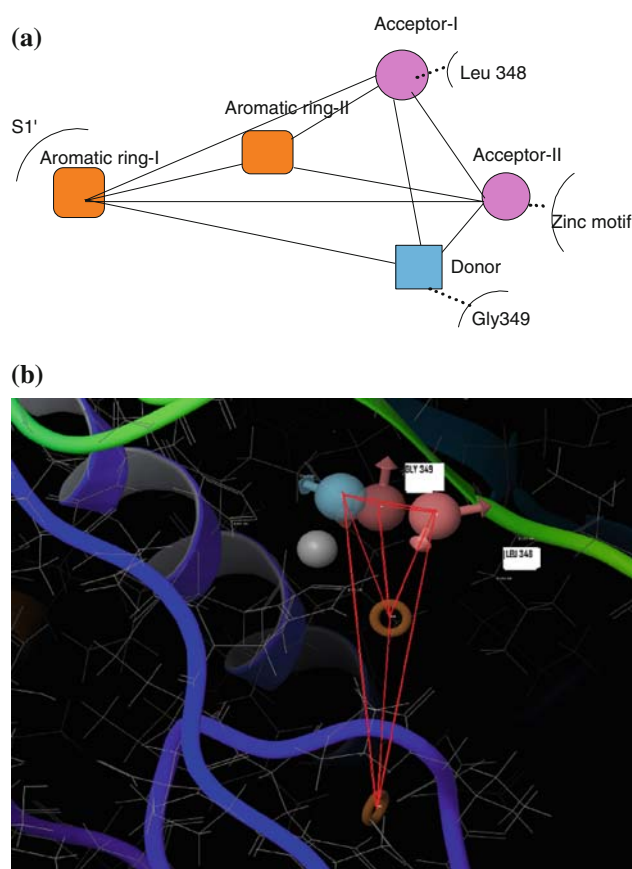


Fig. 5 Mapping of the Pharmacophore features (CPH1) in the active site of TACE. **a** 2D representation of pharmacophoric features interacting with TACE. **b** Interaction of Pharmacophoric features with TACE (chain-B of 2fv5 pdb)

the validity of the developed pharmacophore model (CPH1). Figure 6a–d shows mapping of all four active compounds on CPH1. For IK682 (**78**), the two acceptors mapped on the two carbonyl groups, one present on pyrrolidine ring and the other as a part of hydroxamate group (Fig. 6a). The two aromatic ring features of the pharmacophore, mapped on the central phenyl ring and on the phenyl part of the quinoline ring. The donor feature mapped on the NH of hydroxamate group. Compound **81** (pIC₅₀ = 9.657) reported by Xue et al. [20] is a selective and potent TACE inhibitor. One acceptor feature of the pharmacophore mapped on the carbonyl group of anilido group, and the other acceptor on the carbonyl of hydroxamate group. The aromatic ring features mapped on the central phenyl ring and on the pyridine ring of the quinoline moiety (Fig. 6b). Figure 6c, d show the mapping of compound **82** and compound **83** on CPH1. These studies provide confidence in the applicability of the model and the pharmacophore model (CPH1) so developed could be utilized for in silico screening of any data base for TACE inhibitory activity.

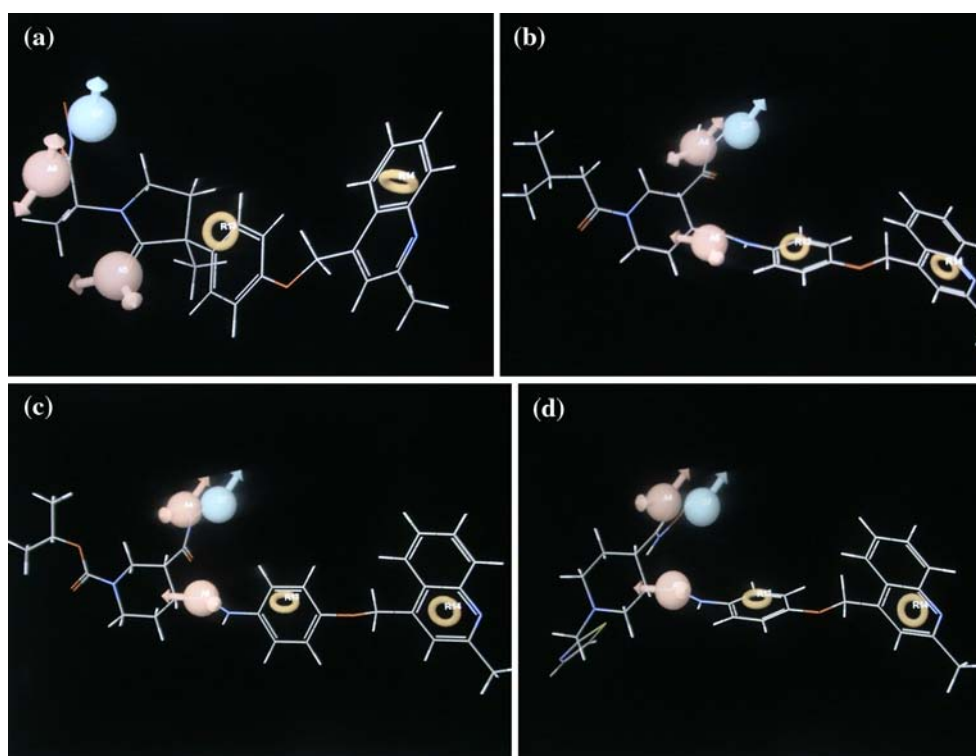


Fig. 6 Mapping of active compounds on CPH1, **a** compound **78**, **b** compound **81**, **c** compound **82**, **d** compound **83**

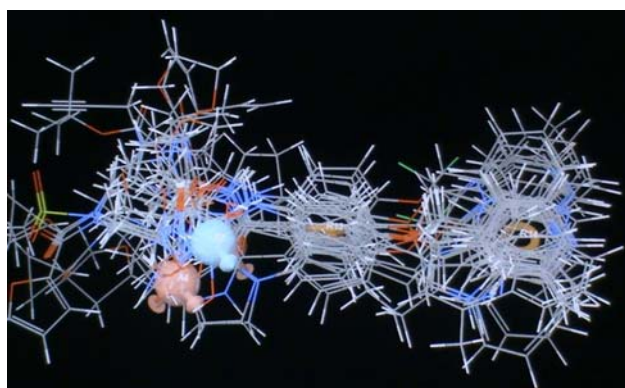


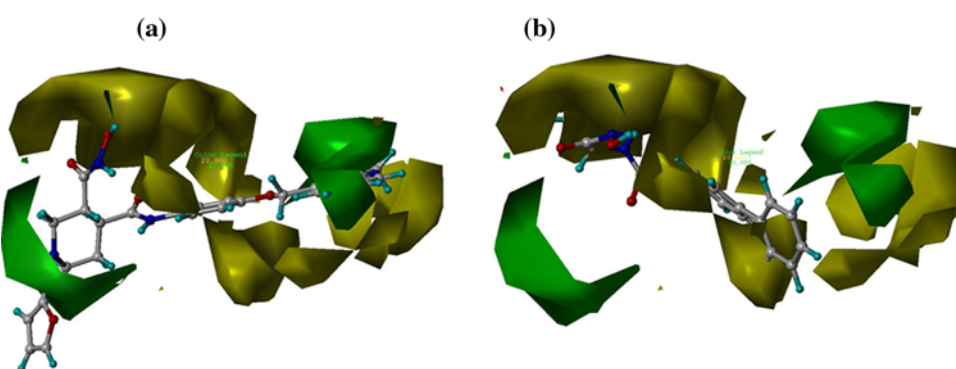
Fig. 7 Common pharmacophore hypothesis 1 (CPH1)-based alignment of TACE inhibitors

The hypothesis CPH1 with two hydrogen bond acceptors (A), one donor group (D), and two aromatic rings (R) as pharmacophoric features was further subjected to CoMFA and CoMSIA studies. Figure 7 shows the alignment of the molecules under study along with CPH1. Efforts were also made to develop a model based on the alignment employing atom/shape-based RMS fitting and RMSD-based database fitting techniques for the lower energy conformers obtained from MULTISEARCH option in SYBYL. However, models derived by using alignment based on lower energy conformers resulted into poor

statistics hence, are not discussed in detail. CPH1-based alignments were considered for further analysis. CoMFA generated a good internal predictive ability ($r_{cv}^2 = 0.594$), a small standard error of estimation (SEE = 0.213) and having predictive r^2 in acceptable range (predictive $r^2 > 0.300$). This model was used to explain SAR and to carry out further analysis, and all the CoMFA contours were generated using this model. The field values generated at each grid point were calculated as the scalar product of the associated QSAR coefficient and the standard deviation of all values in the corresponding column of the data table (STD*COEFF) plotted as the percentage contributions to QSAR equation. The CoMFA steric and electrostatic contour maps are shown in Fig. 8, 9 respectively. The green colour regions indicate areas where steric bulk enhances TACE inhibitory activity, while the yellow contours indicate regions where steric bulk is detrimental for biological activity. Blue colour regions show areas where electro-positive charged groups enhance TACE inhibitory activity, while red regions represent where electronegative charged groups improve the activity. The results of PLS analyses from CoMFA studies are summarized in Table 3.

The CoMSIA analysis was performed using steric, electrostatic, hydrophobic, hydrogen bond donor and acceptor fields. Results of this study are summarized in Table 3. The CoMSIA models showed good correlation and predictive properties. The CoMSIA model with

Fig. 8 The CoMFA steric STDEV*COEFF contour plots of **a** active compound (**58**) and **b** inactive compound (**72**). Sterically favored areas (contribution level 80%) are represented by green polyhedra. Sterically disfavored areas (contribution level 20%) are represented by yellow polyhedra



combination of all the fields yielded a cross-validated $r^2 = 0.456$ with six components, non-cross-validated $r^2 = 0.875$, F-value 130.089 [F05 (06, 60) = 2.254 (Tab)] and predictive $r^2 = 0.421$. The contributions of steric, electrostatic, hydrophobic, hydrogen bond donor and acceptor fields of this model were 20.0, 22.6, 18.2, 22.3 and 17.0% respectively. The CoMSIA model with a combination of steric, electrostatic, and hydrophobic fields yielded the highest cross-validated $r^2 = 0.598$ with six components, non-cross-validated $r^2 = 0.943$, F-value 232.34 [F05 (06, 54) = 2.254 (Tab)] but having poor predictive r^2 i.e. 0.312. The steric, electrostatic and hydrophobic field contributions were 29.7, 29.1 and 41.2%, respectively. Combinations of steric, electrostatic and hydrogen bond donor fields yielded a CoMSIA model with a cross-validated $r^2 = 0.475$ with five components, non-cross-validated

$r^2 = 0.912$, F-value 123.23 [F05 (05, 55) = 2.368 (Tab)] and predictive $r^2 = 0.338$. The steric, electrostatic and hydrogen bond donor contributions were 29.5, 28.2 and 42.3%, respectively. CoMSIA model generated with combination of steric, electrostatic, hydrogen bond acceptor and hydrophobic fields yielded a cross-validated $r^2 = 0.572$ with five components, non-cross-validated $r^2 = 0.974$, F-value 341.79 [F05(05, 55) = 2.368 (Tab)] and excellent predictive $r^2 = 0.529$. The steric, electrostatic and hydrogen bond acceptor and hydrophobic fields of this model were 25.4, 29.2, 20.00 and 25.4%, respectively. The CoMSIA model with this combination (SEAH; Table 3) was considered to be the best model as it has got the best internal as well as external predictive ability. The models generated by various combinations of CoMSIA fields (Table 3) showed moderate to high, internal and external predictions,

Table 3 Summary of CoMFA and CoMSIA results

Descriptors	r_{cv}^2	NC	r_{ncv}^2	SEE	F -value	r_{pred}^2	Contribution (fraction)				
							S	E	A	D	H
CoMFA											
SE	0.594	5	0.936	0.213	285.868	0.419	55.7	44.3	–	–	–
COMSIA											
H ^a	0.498	6	0.960	0.241	220.529	0.150	–	–	–	–	–
D ^b	0.457	3	0.786	0.543	70.981	0.108	–	–	–	–	–
A ^c	0.213	5	0.829	0.512	56.13	0.173	–	–	–	–	–
DA	0.402	2	0.713	0.624	73.201	0.168	–	–	44.4	55.6	–
HD	0.404	5	0.915	0.349	160.053	0.512	–	–	–	51.5	48.5
HA	0.374	5	0.927	0.320	180.724	0.324	–	–	44.0	–	56.0
HDA	0.434	2	0.823	0.572	92.976	0.321	–	–	28.3	35.8	35.9
S ^d ED	0.475	5	0.912	0.412	123.23	0.338	29.5	28.2	–	42.3	–
HSE ^e	0.598	6	0.943	0.242	232.34	0.312	29.7	29.1	–	–	41.2
SEA	0.467	5	0.920	0.370	110.798	0.496	35.5	31.3	33.2	–	–
SEDA	0.545	6	0.975	0.191	356.147	0.354	26.3	27.5	17.0	29.1	–
SEDAH	0.456	6	0.875	0.422	130.089	0.421	20.0	22.6	17.0	22.3	18.2
SEAH ^f	0.572	5	0.974	0.195	341.790	0.529	25.4	29.2	20.0	–	25.4
SEDH	0.509	5	0.921	0.336	173.477	0.429	21.0	20.9	–	29.1	29.0

Bold values indicate the model having the best statistical figures when compared to other developed models

^a Hydrophobic field, ^b Hydrogen bond donor field, ^c Hydrogen bond acceptor field, ^d Steric field, ^e Electrostatic field, ^f Best model for CoMSIA

in which the hydrogen bond donor fields were observed to be dominant over the hydrophobic fields and hydrogen bond acceptor fields. The CoMSIA steric and electrostatic contours (not shown) were positioned similarly to those of the CoMFA model, hence are not discussed. The results of CoMSIA PLS analysis are summarized in Table 3. The CoMSIA model generated from steric and electrostatic fields did not vary both in terms of statistical values and positions of contours, as compared with its CoMFA model and hence are not included in the table. The hydrophobic contour maps of CoMSIA (STDDEV*COEFF) is displayed in Fig. 11.

Graphical interpretation of 3D CoMFA and CoMSIA models

Additional insight into the structural requirements for TACE inhibitory activity could be gained by visualising the 3D-QSAR contour maps. This information can then be used to design new, more potent analogues. A pictorial representation of the contours generated is given in Figs. 8–11. Figures 8 and 9 indicate the CoMFA steric and electrostatic contour maps, respectively, using (1) compound **58** (most active compound) and (2) compound **72** (least active), as a reference structure. In this figure, the green contours represent regions of high steric tolerance (80% contribution), while the yellow contours represent regions of low steric tolerance (20% contribution). The increase in positive charge is favored in blue regions while increase in negative charge is favored in red regions. The steric contour of CoMFA (Fig. 8) shows a green contour enclosing the quinoline ring of the template structure. This indicates that bulky groups here would enhance the TACE inhibitory activity. Good inhibitory potency of **6** (IC_{50} 0.14), **61** (IC_{50} 0.28), **4** (IC_{50} 0.4), **59** (IC_{50} 0.45), **60** (IC_{50} 0.48) and **5** (IC_{50} 0.94) is because of orientation of bulkier groups toward sterically favored green contour. Absence of the bulkier group at this position leads to decrease in the activity, as this could be observed with compounds **72** (IC_{50} 13000), **79**

(IC_{50} 2200), **69** (IC_{50} 887), **68** (IC_{50} 111) and **70** (IC_{50} 97) which have got poor TACE inhibitory activity. The steric contour map of CoMFA also shows a large contour enclosing the piperidine ring of the template molecule where more bulky substitutions are expected to increase the activity. High potency of compounds **6** (IC_{50} 0.14), **61** (IC_{50} 0.28), **59** (IC_{50} 0.45), **10** (IC_{50} 1.0) and **62** (IC_{50} 1.6) is because of orientation of bulkier groups toward the sterically favored green contour. The steric contour map also shows yellow contour near quinoline ring. Here, bulky substituents are not tolerated hence compound **47** (IC_{50} 81), **48** (IC_{50} 1110), **29** (IC_{50} 900), **30** (IC_{50} 294), **24** (IC_{50} 170) and **25** (IC_{50} 150) exhibited low inhibitory activity as quinoline ring of this compound lies in the yellow region. Compound **72** has got the least activity in the series as it occupies the region in the sterically disfavoured area which is clearly evident from Fig. 9.

The electrostatic contours of CoMFA (Fig. 9a) are clearly distributed in three regions i.e. quinoline region, central phenyl ring favouring electropositive substituent groups and red contour surrounding the piperidine ring towards the hydroxamate group of the template molecule where high electron density is expected to increase the activity.

The CoMSIA hydrogen bond acceptor fields (magenta polyhedra) (Fig. 10) indicate regions where hydrogen bond acceptor substituents are favored and red polyhedra indicate disfavored regions. The magenta polyhedron, indicating hydrogen bond acceptor favourable region, is present in the surrounding of piperidine ring where carbonyl groups attached to 1, 3 or 4 positions acts as hydrogen bond acceptors. Thus, hydrogen acceptor atom (an electronegative atom such as fluorine, oxygen, or nitrogen is a hydrogen bond acceptor) substituted at 1, 3 or 4 position of piperidine ring may enhance the TACE inhibitory activity. As for as compound **72** is concerned, the hydrogen bond acceptor group i.e. carbonyl group is projected towards the disfavoured region (red polyhedra) (Fig. 10b) leading to the decrease in its activity.

Fig. 9 The CoMFA electrostatic STDEV*COEFF contour plots of **a** active compound (**58**) and **b** inactive compound (**72**). Positively charged favored areas (contribution level 80%) are represented by blue polyhedron. Negatively charged favored areas (contribution level 20%) are represented by red polyhedra

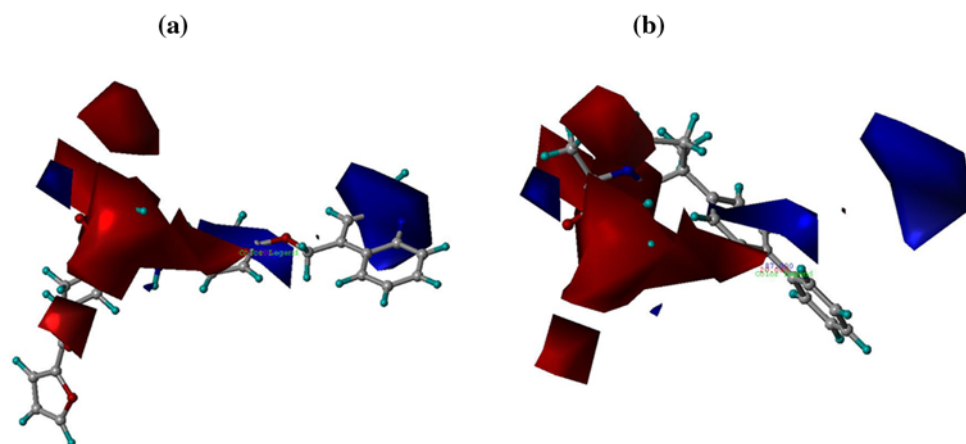


Fig. 10 The CoMSIA hydrogen bond acceptor fields of **a** active compound (**58**) and **b** inactive compound (**72**). *Magenta polyhedra* indicate regions where hydrogen bond acceptor substituents are favored and *red polyhedra* indicate disfavored regions

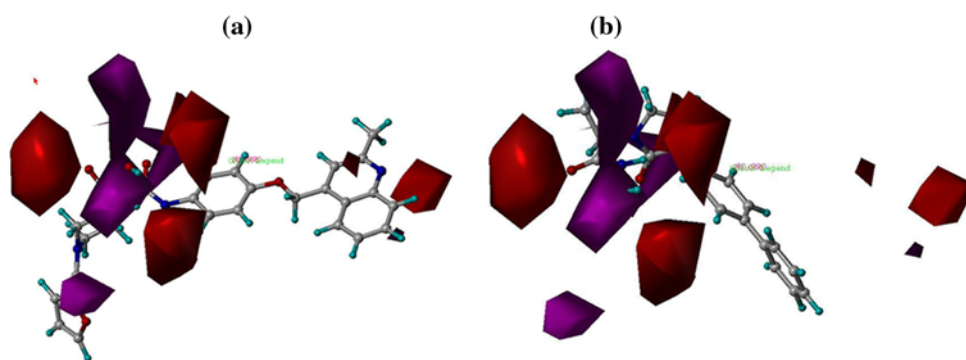
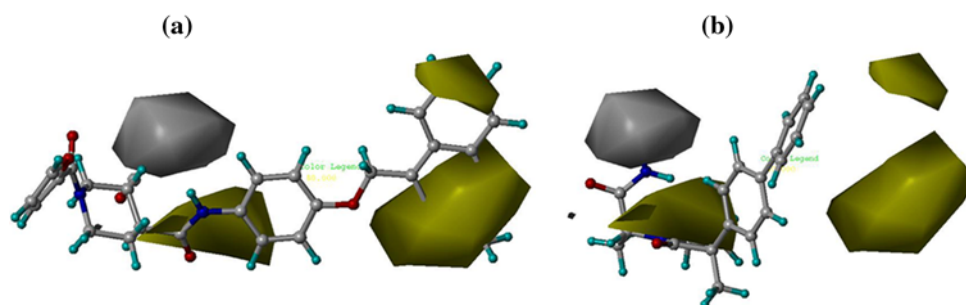


Fig. 11 The CoMSIA hydrophobic fields of **a** active compounds (**58**) and **b** inactive compound (**72**). *Yellow polyhedra* indicate regions where hydrophobic substituents are favored and *white polyhedra* indicate disfavored regions



The CoMSIA hydrophobic fields (yellow polyhedra) (Fig. 11) indicate regions where hydrophobic substituents are favored and white polyhedra indicate disfavored regions. The white disfavored hydrophobic contour (Fig. 11) is observed in the vicinity of hydroxamate group where hydrophobic substituents are detrimental for TACE inhibitory activity. The hydrophobic contours (Fig. 11) show presence of a yellow contour surrounding the quinoline ring indicating that more hydrophobic substituent in this region may improve the biological activity. In Fig. 11a, the quinoline ring present in the compound **58** lies in the favoured region where as in Fig. 11b, biphenyl ring present in compound **72** is not oriented towards the favoured region which could be a probable reason for the difference in the activity of these two compounds.

Conclusion

Different pharmacophore hypotheses were developed for TACE inhibitors using PHASE. A five-point pharmacophore with two hydrogen bond acceptors (A), one hydrogen bond donor (D) and two aromatic rings (R) as pharmacophoric features was associated with high predictive power. Pharmacophore mapping studies provided an insight into the inhibitory potential of different chemotypes as TACE inhibitor. The developed pharmacophoric model was utilized for in silico screening of compounds from a data base for potential TACE inhibitors. Authenticity of model got confirmed when four active and two inactive compounds grafted into the data base from outside, were

correctly identified. Furthermore, the alignment based on the best pharmacophore hypothesis (CPH1) was used as the input for the development of CoMFA and CoMSIA 3D-QSARs. Visualisation of the 3D-CoMSIA model in context of the molecules under study provided details of the structure activity relationship thus providing information regarding structural modifications with which to design analogues with better activity prior to synthesis. In summary, the ligand-based pharmacophore model and the 3D-CoMSIA model presented in this study could be very useful for the in silico data base screening and designing of more potent TACE inhibitors.

Acknowledgments We thank All India Council for Technical Education (A.I.C.T.E), New Delhi, India for financial support [File No. 8023/BOR/RID/RPS-148/2007-08]. Prashant R. Murumkar is thankful to A.I.C.T.E, New Delhi, India for the award of National Doctoral Fellowship [F.NO:1-10/FD/NDF-PG/(41)/2006-07].

References

- Black RA, Rauch CT, Kozlosky CJ, Peschon JJ, Slack JL, Wolfson MF, Castner BJ, Stocking KL, Reddy P, Srinivasan S, Nelson N, Boiani N, Schooley KA, Gerhart M, Davis R, Fitzner JN, Johnson RS, Paxton RJ, March CJ, Cerretti DP (1997) A metalloproteinase disintegrin that releases tumour-necrosis factor- α from cells. *Nature* 385:729–733. doi:10.1038/385729a0
- Vassalli P (1992) The pathophysiology of tumor necrosis factors. *Ann Rev Immunol* 10:411–452. doi:10.1146/annurev.iy.10.040192.002211
- Maini RN, Elliott MJ, Brennan FM, Feldmann M (1995) Beneficial effects of tumour necrosis factor-alpha (TNF-alpha) blockade in rheumatoid arthritis (RA). *Clin Exp Immunol* 101:207–212

4. Elliott MJ, Maini RN, Feldmann M, Long-Fox A, Charles P, Bijl H, Woody JN (1994) Repeated therapy with monoclonal antibody to tumour necrosis factor α (cA2) in patients with rheumatoid arthritis. *Lancet* 344:1125–1127
5. Dixon SL, Smondyrev AM, Rao SN (2006) PHASE: a novel approach to pharmacophore modeling and 3D database searching. *Chem Biol Drug Des* 67:370–372. doi:[10.1111/j.1747-0285.2006.00384.x](https://doi.org/10.1111/j.1747-0285.2006.00384.x)
6. Mutasem O, Taha LA, Dahabiyesh YB, Hiba Z, Suhair S (2008) Combining ligand-based pharmacophore modeling, quantitative structure-activity relationship analysis and in silico screening for the discovery of new potent hormone sensitive lipase inhibitors. *J Med Chem* 51:6478–6494. doi:[10.1021/jm800718k](https://doi.org/10.1021/jm800718k)
7. Maskos K, Fernandez-Catalan C, Huber R, Bourenkov GP, Bartunik H, Ellestad GA, Reddy P, Wolfson MF, Rauch CT, Castner BJ, Davis R, Clarke HR, Petersen M, Fitzner JN, Cerretti DP, March CJ, Paxton RJ, Black RA, Bode W (1998) Crystal structure of the catalytic domain of human tumor necrosis factor- α -converting enzyme. *Proc Natl Acad Sci USA* 95:3408–3412
8. Newton RC, Decicco CP (1999) Therapeutic potential and strategies for inhibiting tumor necrosis factor- α . *J Med Chem* 42:2295–2314. doi:[10.1021/jm980541n](https://doi.org/10.1021/jm980541n)
9. Grootveld M, McDermott M (2003) BMS-561392 (Bristol-Myers Squibb). *Curr Opin Investig Drugs* 4:598–602. PMID: 12833656
10. Mustata GI, Brigo A, Briggs JM (2004) HIV-1 integrase pharmacophore model derived from diverse classes of inhibitors. *Bioorg Med Chem Lett* 14:1447–1454. doi:[10.1016/j.bmcl.2004.01.027](https://doi.org/10.1016/j.bmcl.2004.01.027)
11. Murumkar PR, Giridhar R, Yadav MR (2008) 3D-quantitative structure-activity relationship studies on benzothiadiazepine hydroxamates as inhibitors of tumor necrosis factor- α converting enzyme. *Chem Biol Drug Des* 71:363–373. doi:[10.1111/j.1747-0285.2008.00639.x](https://doi.org/10.1111/j.1747-0285.2008.00639.x)
12. Murumkar PR, Dasgupta SD, Zambre VP, Giridhar R, Yadav MR (2009) Development of predictive 3D-QSAR CoMFA and CoMSIA models for α -aminohydroxamic acid-derived tumor necrosis factor- α converting enzyme inhibitors. *Chem Biol Drug Des* 73:97–107. doi:[10.1111/j.1747-0285.2008.00737.x](https://doi.org/10.1111/j.1747-0285.2008.00737.x)
13. Murumkar PR, Dasgupta SD, Chandani SR, Giridhar R, Yadav MR (2010) Novel TACE inhibitors in drug discovery: a review of patented compounds. *Expert Opin Ther Pat* 20:31–57. doi:[10.1517/13543770903465157](https://doi.org/10.1517/13543770903465157)
14. Dasgupta S, Murumkar PR, Giridhar R, Yadav MR (2009) Current perspective of TACE inhibitors: a review. *Bioorg Med Chem* 17:444–459. doi:[10.1016/j.bmc.2008.11.067](https://doi.org/10.1016/j.bmc.2008.11.067)
15. Dasgupta S, Murumkar PR, Giridhar R, Yadav MR (2009) Studies on novel 2-imidazolidinones and tetrahydropyrimidin-2(1H)-ones as potential TACE inhibitors: design, synthesis, molecular modeling, and preliminary biological evaluation. *Bioorg Med Chem* 17:3604–3617. doi:[10.1016/j.bmc.2009.04.003](https://doi.org/10.1016/j.bmc.2009.04.003)
16. Yadav MR, Dasgupta S, Murumkar PR, Giridhar R (2010) In: Berhardt L (ed) *Advances in medicine and biology*, vol 3. Nova Science, New York (in press)
17. Dixon SL, Smondyrev AM, Knoll EH, Rao SN, Shaw DE, Friesner RA (2006) PHASE: a new engine for pharmacophore perception, 3D QSAR model development, and 3D database screening: 1 methodology and preliminary results. *Computer-Aided Mol Des* 20:647–667. doi:[10.1007/s10822-006-9087-6](https://doi.org/10.1007/s10822-006-9087-6)
18. Duan JJ, Chen L, Wasserman ZR, Lu Z, Liu RQ, Covington MB, Qian M, Hardman KD, Magolda RL, Newton Christ DD, Wexler RR, Decicco CP (2002) Discovery of γ -lactam hydroxamic acids as selective inhibitors of tumor necrosis factor- α converting enzyme: design, synthesis, and structure-activity relationships. *J Med Chem* 45:4954–4957. doi:[10.1021/jm0255670](https://doi.org/10.1021/jm0255670)
19. Duan JJ, Lu Z, Xue C, He X, Seng JL, Roderick JJ, Wasserman ZR, Liu R, Covington MB, Magolda RL, Newton RC, Trzaskos JM, Decicco CP (2003) Discovery of N-Hydroxy-2-(2-oxo-3-pyrrolidinyl)acetamides as potent and selective inhibitors of tumor necrosis factor- α converting enzyme (TACE). *Bioorg Med Chem Lett* 13:2035–2040. doi:[10.1016/S0960-894X\(03\)00313-5](https://doi.org/10.1016/S0960-894X(03)00313-5)
20. Xue C, He X, Roderick J, Corbett RL, Duan JJ, Liu RQ, Covington MB, Qian M, Ribadeneira MD, Vaddi K, Christ DD, Newton RC, Trzaskos JM, Magolda RL, Wexler RR, Decicco CP (2003) Rational design, synthesis and structure-activity relationships of a cyclic succinate series of TNF- α converting enzyme inhibitors. Part 2: lead optimization. *Bioorg Med Chem Lett* 13:4299–4304. doi:[10.1016/j.bmcl.2003.09.057](https://doi.org/10.1016/j.bmcl.2003.09.057)
21. Gilmore JL, King Bryan W, Asakawa N, Harrison K, Tebben A, Sheppeck JE II, Liu RQ, Covington M, Duan JJW (2007) Synthesis and structure-activity relationship of a novel, non-hydroxamate series of TNF- α converting enzyme inhibitors. *Bioorg Med Chem Lett* 17:4678–4682. doi:[10.1016/j.bmcl.2007.05.100](https://doi.org/10.1016/j.bmcl.2007.05.100)
22. Duan JJW, Lu Z, Wasserman ZR, Liu R, Covington MB, Decicco CP (2005) Non-hydroxamate 5-phenylpyrimidine-2, 4, 6-trione derivatives as selective inhibitors of tumor necrosis factor- α converting enzyme. *Bioorg Med Chem Lett* 15:2970–2973. doi:[10.1016/j.bmcl.2005.04.039](https://doi.org/10.1016/j.bmcl.2005.04.039)
23. Gilmore JL, King BW, Harris C, Maduskuie T, Mercer SE, Liu R, Covington MB, Qian M, Ribadeneira MD, Vaddi K, Trzaskos JM, Newton RC, Decicco CP, Duan JJW (2006) Synthesis and structure-activity relationship of a novel, achiral series of TNF- α converting enzyme inhibitors. *Bioorg Med Chem Lett* 16:2699–2704. doi:[10.1016/j.bmcl.2006.02.015](https://doi.org/10.1016/j.bmcl.2006.02.015)
24. Sheppeck JE, Gilmore JL, Yang A, Wasserman ZR, Decicco CP, Duan JJW (2007) A molecular modeling analysis of novel non-hydroxamate inhibitors of TACE. *Bioorg Med Chem Lett* 17:1408–1412. doi:[10.1016/j.bmcl.2006.11.082](https://doi.org/10.1016/j.bmcl.2006.11.082)
25. Sheppeck JE, Gilmore JL, Yang A, Chen X, Xue CB, Roderick J, Liu RQ, Covington MB, Decicco CP, Duan JJW (2007) Discovery of novel hydantoins as selective non-hydroxamate inhibitors of tumor necrosis factor- α converting enzyme (TACE). *Bioorg Med Chem Lett* 17:1413–1417. doi:[10.1016/j.bmcl.2006.11.089](https://doi.org/10.1016/j.bmcl.2006.11.089)
26. Ott GR, Asakawa N, Lu Z, Liu RQ, Covington MB, Vaddi K, Quin M, Newton RC, Christ D, Traskos JM, Decicco CP, Duan JJW (2008) α , β -Cyclic- β -benzamido hydroxamic acids: novel templates for the design, synthesis, and evaluation of selective inhibitors of TNF- α converting enzyme (TACE). *Bioorg Med Chem Lett* 18:694–699. doi:[10.1016/j.bmcl.2007.11.059](https://doi.org/10.1016/j.bmcl.2007.11.059)
27. Ott GR, Asakawa N, Liu RQ, Covington MB, Vaddi K, Newton RC, Traskos JM, Christ DD, Galya L, Cholz T, Marshall W, Duan JJW (2008) α , β -Cyclic- β -benzamido hydroxamic acids: novel oxaspiro[4.4]nonane templates for the discovery of potent, selective, orally bioavailable inhibitors of tumor necrosis factor- α converting enzyme (TACE). *Bioorg Med Chem Lett* 18:1288–1292. doi:[10.1016/j.bmcl.2008.01.030](https://doi.org/10.1016/j.bmcl.2008.01.030)
28. Lu Z, Ott GR, Anad R, Liu RQ, Covington MB, Vaddi K, Qian M, Newton RC, Christ DD, Traskos JM, Duan JJW (2008) Potent, selective, orally bioavailable inhibitors of tumor necrosis factor- α converting enzyme (TACE): discovery of indole, benzofuran, imidazopyridine and pyrazolopyridine P1' substituents. *Bioorg Med Chem Lett* 18:1958–1962. doi:[10.1016/j.bmcl.2008.01.120](https://doi.org/10.1016/j.bmcl.2008.01.120)
29. Ott GR, Asakawa N, Lu Z, Anad R, Liu RQ, Covington MB, Vaddi K, Qian M, Newton RC, Christ DD, Traskos JM, Duan JJW (2008) Potent, exceptionally selective, orally bioavailable inhibitors of TNF- α converting enzyme (TACE): novel 2-substituted-1H-benzo[d]imidazol-1-yl)methyl)benzamide P1' substituents. *Bioorg Med Chem Lett* 18:1577–1582. doi:[10.1016/j.bmcl.2008.01.075](https://doi.org/10.1016/j.bmcl.2008.01.075)
30. SYBYL 7.0 (1699) Tripos Inc., 1st Louis
31. <http://www.expasy.org/blast>
32. Entry A7Y1V1: <http://www.expasy.org/uniprot/A7Y1V1>